An Optimal Regulation of Fluxes Dictates Microbial Growth In and Out of Steady-State

Griffin Chure and Jonas Cremer

Department of Biology, Stanford University, Stanford, CA, USA.

gchure@stanford.edu, jbcremer@stanford.edu

August 11, 2022

Abstract

Effective coordination of cellular processes is critical to ensure the competitive growth of microbial organisms. Pivotal to this coordination is the appropriate partitioning of cellular resources between protein synthesis via translation and the metabolism needed to sustain it. Here, we extend a low-dimensional allocation model to describe the dynamic control of this resource partitioning. At the core of this regulation is the optimal coordination of metabolic and translational fluxes, mechanistically achieved via the perception of charged- and uncharged-tRNA turnover. An extensive comparison with $\approx$ 60 data sets from *Escherichia coli* establishes this regulatory mechanism's biological veracity and demonstrates that a remarkably wide range of growth phenomena in and out of steady state can be predicted with quantitative accuracy. This predictive power, achieved with only a few biological parameters, cements the preeminent importance of optimal flux regulation across conditions and establishes low-dimensional allocation models as an ideal physiological framework to interrogate the dynamics of growth, competition, and adaptation in complex and ever-changing environments.

Introduction

Growth and reproduction is central to life. This is particularly true of microbial organisms where the ability to quickly accumulate biomass is critical for competition in ecologically diverse habitats. Understanding which cellular processes are key in defining growth has thus become a fundamental goal in the field of microbiology. Pioneering physiological and metabolic studies throughout the 20th century laid the groundwork needed to answer this question [1–11], with the extensive characterization of cellular composition across growth conditions at both the elemental [12–14] and molecular [7, 8, 15, 16] levels showing that the dry mass of microbial cells is primarily composed of proteins and RNA. Seminal studies further revealed that the cellular RNA content is strongly correlated with the growth rate [7, 8, 17], an observation which has held for many microbial species [18]. As the majority of RNA is ribosomal, these observations suggested that protein synthesis via ribosomes is a major determinant of biomass accumulation in nutrient replete conditions [19–21]. Given that the cellular processes involved in biosynthesis, particularly those of protein synthesis, are well conserved between species and domains [22–24], these findings have inspired hope that fundamental principles of microbial growth can be found despite the enormous diversity of microbial species and the variety of habitats they occupy.

The past decade has seen a flurry of experimental studies further establishing the importance of protein synthesis in defining growth. Approaches include modern "-omics" techniques with molecular-level resolution [25–38], measurements of many core physiological processes and their coordination [38–46], and the perturbation of major cellular processes like translation [39, 47–49]. Together, these studies advanced a more thorough description of how cells allocate their ribosomes to the synthesis of different proteins depending on their metabolic state and the environmental conditions they encounter, called *ribosomal allocation*. Tied to the experimental studies, theoretical *ribosomal allocation models* have further been formulated to dissect how ribosomal allocation influences growth [31, 32, 49–56, 56–64] (see Appendix 1 for a detailed overview of these approaches). Of particular note is an

array of low-dimensional models which have been developed to describe growth phenomena in varied conditions and physiological limits that rely on only a few parameters [49, 50, 52, 55, 57, 58, 64–66]. The shared minimalism of these models suggests that a single, self-consistent framework can by synthesized to rationalize the fundamental aspects of growth in both static and dynamic environments.

In this work, we build on these low-dimensional allocation models [52,55,60,61,65] and the results from dozens of experimental studies to synthesize a self-consistent and quantitatively predictive description of resource allocation and growth. At the core of our model is the dynamic reallocation of resources between the translational and metabolic machinery, which is sensitive to the metabolic state of the cell. We demonstrate how "optimal allocation"—meaning, an allocation towards ribosomes which contextually maximizes the steady-state growth rate—emerges when the flux of amino acids through translation to generate new proteins and the flux of uncharged-tRNA through metabolism to provide charged-tRNA required for translation are mutually maximized, given the environmental conditions and corresponding physiological constraints. This regulatory scheme, which we term *flux-parity regulation*, can be mechanistically achieved by a global regulator (e.g., guanosine tetraphosphate, ppGpp, in bacteria) capable of simultaneously measuring the turnover of charged- and uncharged-tRNA pools and routing protein synthesis. The explanatory power of the flux-parity regulation circuit is confirmed by extensive comparison of model predictions with ≈ 60 data sets from *Escherichia coli*, spanning more than half a century of studies using varied methodologies. This comparison demonstrates that a simple argument of flux-sensitive regulation is sufficient to predict bacterial growth phenomena in and out of steady-state and across diverse physiological perturbations. The accuracy of the predictions coupled with the minimalism of the model establishes the optimal regulation and cements the centrality of protein synthesis in defining microbial growth. The mechanistic nature of the theory—predicated on a minimal set of biologically meaningful parameters—provides a low-dimensional framework that can be used to explore complex phenomena at the intersection of physiology, ecology, and evolution without requiring extensive characterization of the myriad biochemical processes which drive them.

Results

A simple allocation model describes translation-limited growth

We begin by formulating a simplified model of growth which follows the flow of mass from nutrients in the environment to biomass by building upon and extending the general logic of low-dimensional resource allocation models [39, 47, 50, 52, 55]. Specifically, we focus on the accumulation of *protein* biomass, as protein constitutes the majority of microbial dry mass [67, 68] and peptide bond formation commonly accounts for $\approx 80\%$ of the cellular energy budget [33, 69]. Furthermore, low-dimensional allocation models utilize a simplified representation of the proteome where proteins can be categorized into only a few functional classes [48, 50, 52, 54, 61]. In this work, we consider proteins to be either ribosomal (i.e. directly involved in peptide bond formation using charged-tRNAs), metabolic (i.e. enzymes catalyzing synthesis of charged-tRNA molecules from environmental nutrients), or being involved in all other biological processes (e.g. lipid synthesis, DNA replication, and chemotaxis) [47, 48, 50, 52] (Supplementary Figure 1). Simple allocation models further do not distinguish between different cells but only consider the overall turnover of nutrients and biomass. To this end, we explicitly consider a well-mixed batch culture growth as reference scenario where the nutrients are considered to be in abundance. This low-dimensional view of living matter may at first seem like an unfair approximation, ignoring the decades of work interrogating the multitudinous biochemical and biophysical processes of cell-homeostasis and growth [48, 51, 59, 70, 71]. However, at least in nutrient replete conditions, many of these processes appear not to impose a fundamental limit on the rate of growth in the manner that protein synthesis does [33]. In Appendix 2, we discuss this along with other simplifications in more detail.

To understand protein synthesis and biomass growth within the low-dimensional allocation framework, consider the flux diagram (Fig. 1(A), [31, 33, 50, 52, 55]) showing the masses of the three protein classes, precursors which are required for protein synthesis (e.g. charged-tRNA molecules), nutrients which are required for the synthesis of precursors, and the corresponding fluxes through the key biochemical processes (arrows). This diagram emphasizes that growth is autocatalytic in that the synthesis of ribosomes is undertaken by ribosomes which imposes a strict speed limit on growth [33, 72, 73]. While this may imply that the rate of growth monotonically increases with

increasing ribosome abundance, it is important to remember that metabolic proteins are needed to supply the ribosomes with the precursors needed to form peptide bonds. Herein lies the crux of ribosomal allocation models: the abundance of ribosomes is constrained by the need to synthesize other proteins and growth is a result of how new protein synthesis is partitioned between ribosomal, metabolic, and other proteins. How is this partitioning determined, and how does it affect growth?

To answer these questions, we must understand how these different fluxes interact at a quantitative level and thus must mathematize the biology underlying the boxes and arrows in Fig. 1(A). Taking inspiration from previous models of allocation [47, 50, 52, 55, 61], we enumerate a minimal set of coupled differential equations which captures the flow of mass through metabolism and translation [Fig. 1(C)]. While we present a step-by-step introduction of this model in Appendix 3, we here focus on a summary of the underlying biological intuition and implications of the approach.

We begin by codifying the assertion that protein synthesis is key in determining growth. The synthesis of new total protein mass M depends on the total proteinaceous mass of ribosomes M_{Rb} present in the system and their corresponding average translation rate γ [Fig. 1(B, i)]. As ribosomes rely on precursors to work, it is reasonable to assert that this translation rate must be dependent on the concentration of precursors c_{pc} such that $\gamma \equiv \gamma(c_{pc})$ [52, 55], for which a simple Michaelis-Menten relation is biochemically well motivated [Fig. 1(B, ii)]. The standing precursor concentration c_{pc} is set by a combination of processes [Fig. 1(B, iii)], namely the production of new precursors through metabolism (synthesis), their degradation through translation (consumption), and their dilution as the total cell volume grows. The synthetic process is driven by the abundance of metabolic proteins M_{Mb} in the system and the average metabolic rate ν at which they convert nutrients into charged-tRNAs. While this rate is in general dependent on the concentration of nutrients in the environment (Supplementary Figure 2 and Appendix 3, we here focus on a growth scenario in which nutrient concentrations are saturating. In such a scenario, metabolism operates at a nutrient-specific maximal metabolic rate $\nu \equiv \nu_{max}$. Finally, the relative magnitude of the ribosomal, metabolic, and "other" protein masses is dictated by ϕ_{Rb}, ϕ_{Mb}, and ϕ_O, three *allocation parameters* which range between 0 and 1 and follow the constraint $\phi_{Rb} + \phi_{Mb} + \phi_O = 1$ to describe the allocation of total protein synthesis. Together, these equations provide a full mathematization of the mass flow diagram shown in Fig. 1 (A).

For constant allocation parameters (ϕ_R^*, ϕ_M^*) a steady-state regime emerges from this system of differential equation. Particularly, the precursor concentration is stationary in time ($c_{pc} = c_{pc}^*$), meaning the rate of synthesis is exactly equal to the rate of consumption and dilution. Furthermore, the translation rate $\gamma(c_{pc}^*)$ is constant during steady-state growth and the mass-abundances of ribosomes and metabolic proteins are equivalent to the corresponding allocation parameters, e.g. $\frac{M_{Rb}}{M} \equiv \phi_{Rb}^*$. As a consequence, biomass is increasing exponentially $\frac{dM}{dt} = \lambda M$, with the growth rate $\lambda = \gamma(c_{pc}^*)\phi_{Rb}^*$. The emergence of a steady state and analytical solutions describing steady growth are further discussed in Supplementary Figures 2 and 3. Notably, dilution is important to obtain a steady state as has been highlighted previously by Giordano *et al.* [55] and Dourado *et al.* [61] but is often neglected (Appendix 6).

Fig. 1 (C) and (D) show how the steady-state growth rate λ and translation rate $\gamma(c_{pc}^*)$ are dependent on the allocation towards ribosomes ϕ_{Rb}^*. The figures also show the dependence on the metabolic rate ν_{max} which we here assert to be a proxy for the "quality" of the nutrients in the environment. The non-monotonic dependence of the steady-state growth rate on the ribosome allocation and the metabolic rate poses a critical question: What biological mechanisms determine the allocation towards ribosomes in a particular environment and what criteria must be met for the allocation to ensure efficient growth?

Different Strategies for Regulation of Allocation Predicts Different Phenomenological Behavior

While cells might employ many different ways to regulate allocation, we here consider three specific allocation scenarios to illustrate the importance of allocation on growth. These candidate scenarios either strictly maintain the total ribosomal content (scenario I), maintain a high rate of translation (scenario II), or optimize the steady-state growth rate (scenario III). We derive analytical solutions for these scenarios [Fig. 1(E) and Appendix 7], and ultimately compare these predictions to observations with *Escherichia coli*.

The simplest and perhaps most näive regulatory scenario is one in which the allocation towards ribosomes is

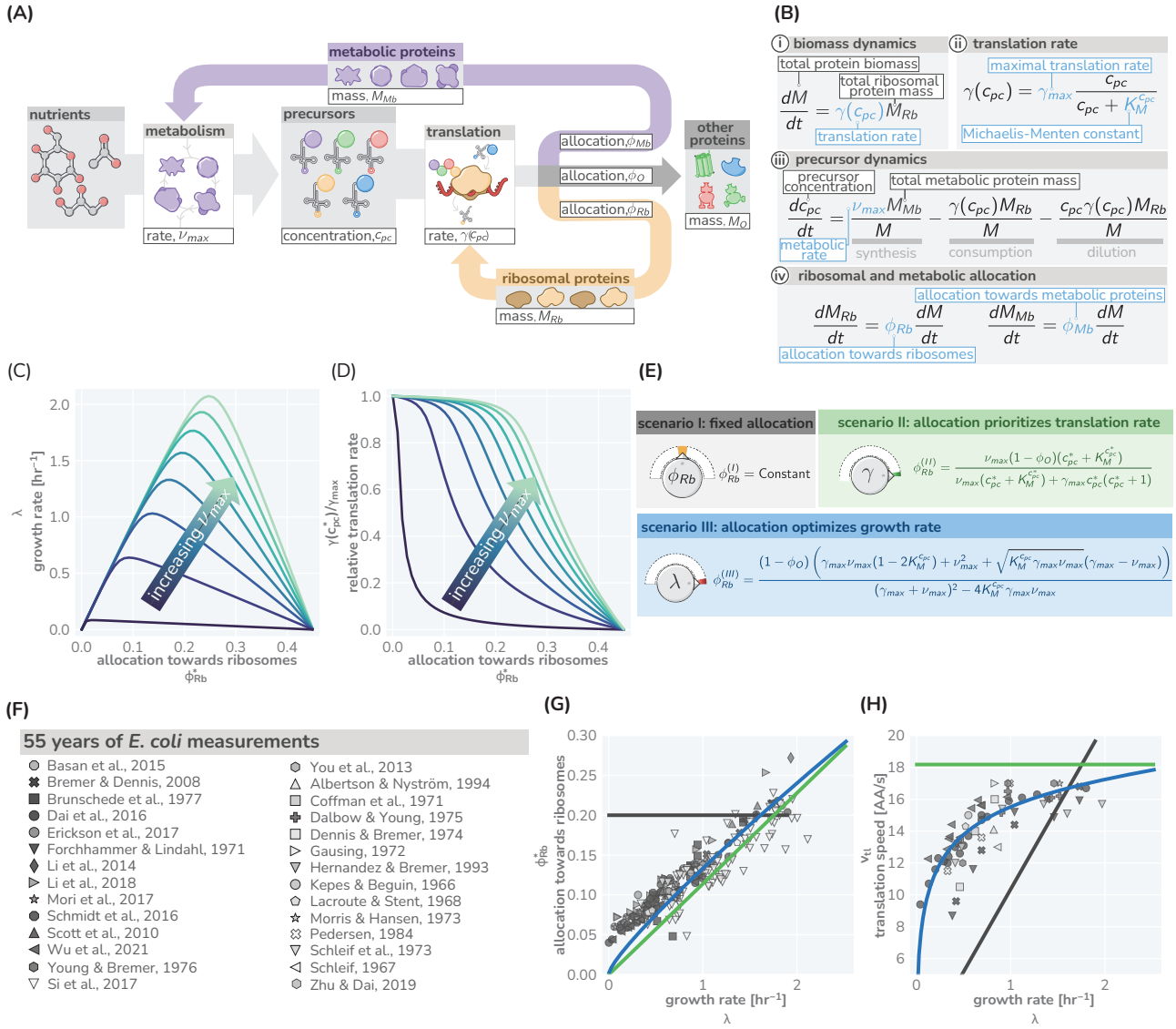

Figure 1: A simple model of ribosomal allocation and hypothetical regulatory strategies. (A) The flow of mass through the self-replicating system. Biomolecules and biosynthetic processes are shown as grey and white boxes, respectively. Nutrients in the environment passed through cellular metabolism to produce "precursor" molecules, here diagrammed as charged-tRNA molecules. These precursors are consumed through the process of translation to produce new protein biomass, either as metabolic proteins (purple arrow), ribosomal proteins (gold arrow), or "other" proteins (gray arrow). The mathematical symbols as used in the simplistic ribosomal allocation model are indicated. (B) Annotated equations of the model with key parameters highlighted in blue. An interactive figure where these equations can be numerically integrated is provided on paper website. The steady-state values of (C) the growth rate λ and (D) the relative translation rate $\gamma(c_{pc}^*)/\gamma_{max}$, are plotted as functions of the allocation towards ribosomes for different metabolic rates (colored lines). (E) Analytical solutions for candidate scenarios for regulation of ribosomal allocation with fixed allocation, allocation to prioritize translation rate, and allocation to optimal growth rate highlighted in grey, green, and blue respectively. (F) A list of collated data sets of *E. coli* ribosomal allocation and translation speed measurements spanning 55 years of research. Details regarding these sources and method of data collation is provided in Table S1. A comparison of the observations with predicted growth-rate dependence of ribosomal allocation (G) and translation speeds (H) for the three allocation strategies. An interactive version of the panels allowing the free adjustment of parameters is available on the associated paper website (`cremerlab.github.io/flux_parity`).

completely fixed and independent of the environmental conditions. This strategy [scenario I in Fig. 1(E, grey)] represents a locked-in physiological state where a specific constant fraction of all proteins is ribosomal. This imposes a strict speed-limit for growth when all ribosomes are translating close to their maximal rate, $\gamma(c_{pc}^*) \approx \gamma_{max}$. If the fixed allocation is low (for example, $\phi_{Rb}^{(I)} = 0.2$), then this speed-limit could be reached at moderate metabolic rates.

A more complex regulatory scenario is one in which the allocation towards ribosomes is adjusted to prioritize the

translation rate. This strategy [scenario II in Fig. 1(E, green)] requires that the ribosomal allocation is adjusted such that a constant internal concentration of precursors c_{pc}^* is maintained across environmental conditions, irrespective of the metabolic rate. In the case where this standing precursor concentration is large ($c_{pc}^* \gg K_M^{c_{pc}}$), all ribosomes will be translating close to their maximal rate.

The third and final regulatory scenario is one in which the allocation towards ribosomes is adjusted such that the steady-state growth rate is maximized. The analytical solution which describes this scenario [scenario III in Fig. 1(E)] resembles previous analytical solutions [55, 61]. More illustratively, the strategy can be thought of as one in which the allocation towards ribosomes is tuned across conditions such that the observed growth rate rests at the peak of the curves in Fig. 1(E). Notably, this does not imply that the translation rate is constantly high across conditions (as in scenario II). Rather, the translation rate is also adjusted and approaches its maximal value γ_{max} only in very rich conditions (high metabolic rates). All allocation scenarios and their consequence on growth are discussed in further detail in Supplementary Figure 4 and the corresponding interactive figure on the paper website.

E. coli Regulates Its Ribosome Content to Optimize Growth

Thus far, our modeling of microbial growth has remained "organism agnostic" without pinning parameters to the specifics of any one microbe's physiology. To probe the predictive power of this simple allocation model and test the plausibility of the three different strategies for regulation of ribosomal allocation, we performed a systematic and comprehensive survey of data from a vast array quantitative studies of the well characterized bacterium *E. coli*. This analysis, consisting of 26 studies spanning 55 years of research (listed in Supplemental Table 2) using varied experimental methods, goes well beyond previous attempts to compare allocation models to data [47, 48, 53–55, 57, 60, 60–63, 65].

These data, shown in Fig. 1(F - H, markers), present a highly-consistent view of *E. coli* physiology where the allocation towards ribosomes (equivalent to ribosomal mass fraction in steady-state balanced growth) and the translation rate demonstrate a strong dependence on the steady-state growth rate in different carbon sources. The pronounced correlation between the allocation towards ribosomes and the steady-state growth rate immediately rules out scenario I, where allocation is constant, as a plausible regulatory strategy used by *E. coli*, regardless of its precise value. Similarly, the presence of a dependence of the translation speed on the growth rate rules out scenario II, where the translation rate is prioritized across growth rates and maintained at a constant value. The observed phenomenology for both the ribosomal allocation *and* the translation speed is only consistent with the logic of regulatory scenario III where the allocation towards ribosomes is tuned to optimize growth rate.

This logic is quantitatively confirmed when we compute the predicted dependencies of these quantities on the steady-state growth rate for the three scenarios diagrammed in Fig. 1(E) based on literature values for key parameters (outlined in Supplemental Table 1). Deviations from the prediction for scenario III are only evident for the ribosomal content at very slow growth ($\lambda \leq 0.5$ hr^{-1}) which are hardly observed in any ecologically relevant conditions and can be attributed to additional biological and experimental factors, including protein degradation [74], ribosome inactivation [39, 42], and cultures which have not yet reached steady state, factors we discuss in Appendix 8.

Importantly, the agreement between theory and observations works with a minimal number of parameters and does not require the inclusion of fitting parameters. All fixed model parameters such as the maximum translation rate γ_{max} and the Michaelis-Menten constant for translation $K_M^{c_{pc}}$, have distinct biological meaning and can be either directly measured or inferred from data (a list is provided in Supplementary Table 1). Furthermore, we discuss the necessity of other parameters such as the "other protein sector" ϕ_O (Appendix 9), its degeneracy with the maximum metabolic rate ν_{max}, and inclusion of ribosome inactivation and minimal ribosome content (Appendix 8). We furthermore provide an interactive figure on the paper website where the parametric sensitivity of these regulatory scenarios and the agreement/disagreement with data can be directly explored. Notably there is no combination of parameter values that would allow scenario I or II to adequately describe both the ribosomal allocation and translation speed as a function of growth rate. Notably, our findings are in line with a recent higher-dimensional modeling study [60] which, based on the optimization of a reaction network with > 200 components, rationalized the variation in translation speed with growth as a manifestation of efficient protein synthesis. Together, these results confirm that scenario III can accurately describe observations over a very broad range of conditions, in strong

support of the popular but often questioned presumption that *E. coli* optimally tunes its ribosomal content to promote fast growth [49, 55, 65].

In Appendix 11, we present a similar analysis for *Saccharomyces cerevisiae* which, in line with previous studies [34–37], suggests that this eukaryote likely follows a similar optimal allocation strategy, although data for ribosomal content and the translation reate is scarce. The strong correlation between ribosome content and growth rate has further been reported for other microbial organisms in line with an optimal allocation [18, 38, 45, 75], though the absence of translation rate measurements precludes confirmation. An interesting exception is the methanogenic archaeon *Methanococcus maripaludis* which appears to maintain constant allocation, in agreement with scenario I [76]. The presented analysis thus suggests that *E. coli* and possibly many other microbes closely follow an optimal ribosome allocation behavior to support efficient growth. Moreover, the good agreement between experiments and data establishes that a simple low-dimensional allocation model can describe growth with notable quantitative accuracy. However, this begs the question: how do cells coordinate their complex machinery to ensure optimal allocation?

Optimal Allocation Results From a Mutual Maximization of Translational and Metabolic Flux

To optimize the steady-state growth rate, cells must have some means of coordinating the flow of mass through metabolism and protein synthesis. In the ribosomal allocation model, this reduces to a regulatory mechanism in which the allocation parameters (ϕ_{Rb} and ϕ_{Mb}) are dynamically adjusted such that the metabolic flux to provide new precursors ($\nu\phi_{Mb}$) and translational flux to make new proteins ($\gamma\phi_{Rb}$, equivalent to the steady-state growth rate λ) are not only equal, but are mutually maximized. Such regulation therefore requires a mechanism by which both the metabolic and translational flux can be simultaneously sensed.

Thus far, we have referred to the end-product of metabolism as ambiguous "precursors" which are used by ribosomes to create new proteins. In reality, these precursors are tRNAs charged with their cognate amino acids. One can think of metabolism as a two-step process where (i) an amino acid is synthesized from environmental nutrients and (ii) an amino acid is attached to the appropriate uncharged-tRNA. As we assume that nutrients are in excess in the environment, we make the approximation that the metabolic rate ν is dependent solely on the uncharged-tRNA concentration $\nu(\text{tRNA}^u)$. This enforces some level of regulation of metabolism; if the uncharged tRNA concentration is too low, the rate of metabolism slows and does not add to the already large pool of charged tRNA. But when charged-tRNA is available, translation occurs at a rate $\gamma(\text{tRNA}^c)$, forming new protein biomass and converting a charged-tRNA back to an uncharged state. This process is shown by grey arrows in Fig. 2(A).

To describe the state-dependent adjustment of the allocation parameters (ϕ_{Rb} and ϕ_{Mb}), we further include in this feedback loop a regulatory system we term a "flux-parity regulator" [Fig. 2(A), red], which controls the allocation parameters in response to relative changes in the concentrations of the two tRNA species. Together, the arrows in Fig. 2 represents a more fine-grained view of a proteinaceous self replicating system, yet maintains much of the structural minimalism of the simple ribosomal allocation model without requiring explicit consideration of different types of amino acids [65], inclusion of their myriad synthesis pathways [60], or reliance on observed phenomenology [42].

The boxes and arrows of Fig. 2(A) can be mathematized to arrive at a handful of ordinary differential equations [Fig. 2(B)] structurally similar to those in Fig. 1(B). At the center of this model is the ansatz that the ribosomal allocation ϕ_{Rb} is dependent on the ratio of charged- and uncharged-tRNA pools and has the form

$$\phi_{Rb}\left(\frac{\text{tRNA}^c}{\text{tRNA}^u}\right) = (1-\phi_O)\frac{\frac{\text{tRNA}^c}{\text{tRNA}^u}}{\frac{\text{tRNA}^c}{\text{tRNA}^u}+\tau}, \tag{1}$$

where the ratio $\frac{\text{tRNA}^c}{\text{tRNA}^u}$ represents the "charging balance" of the tRNA and τ is a dimensionless "sensitivity parameter" which defines the charging balance at which the allocation towards ribosomes is half-maximal. Additionally, we make the assertion that the synthesis rate of new uncharged-tRNA via transcription κ is coregulated with ribosomal

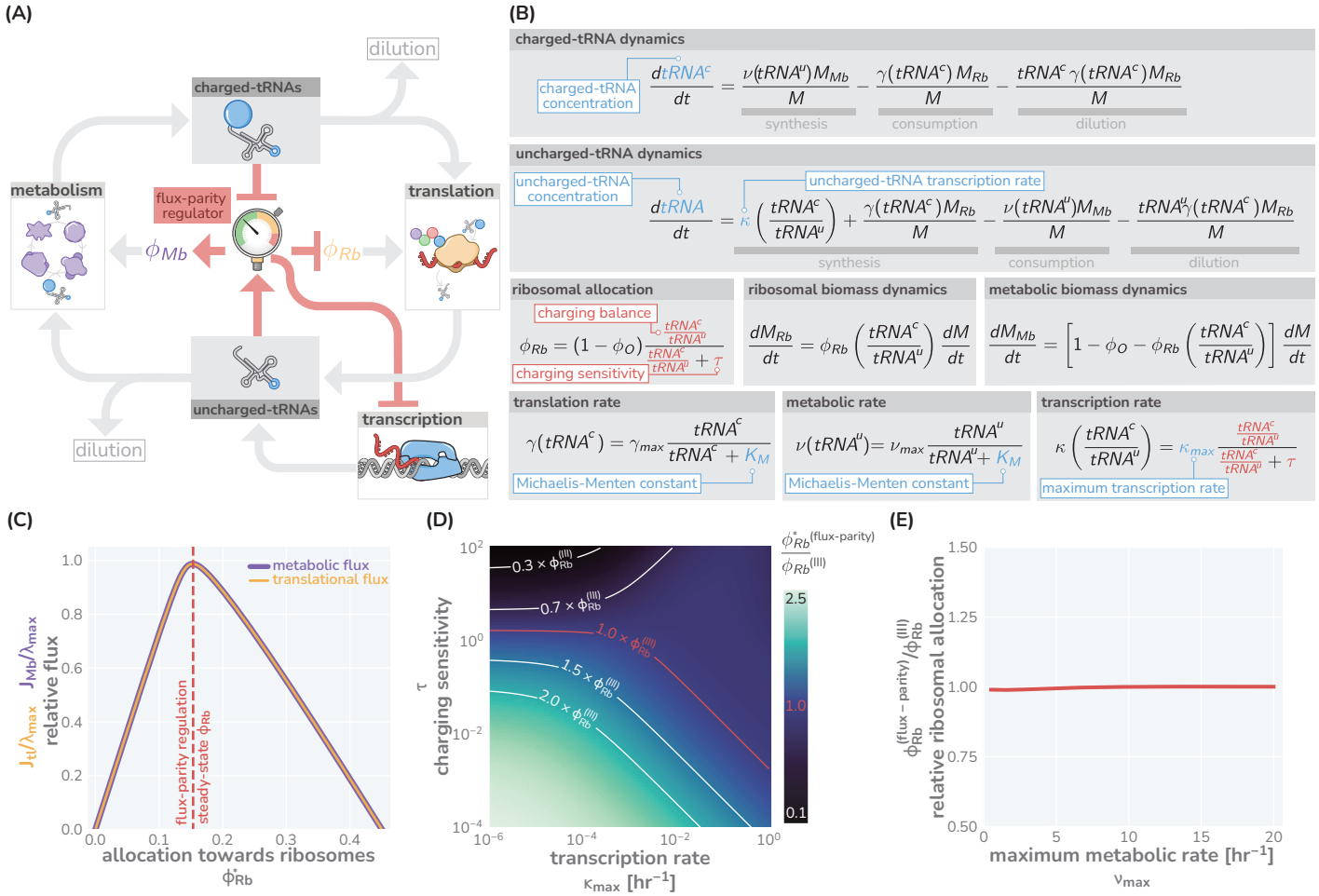

Figure 2: The regulation of ribosome allocation via a flux-sensing mechanism. (A) A circuit diagram of interactions between metabolic and translational fluxes with flux-parity regulatory connections highlighted in red. The fluxes are connected via a positive feedback loop through the generation of mutual starting materials (uncharged- or charged-tRNAs, respectively). The rates of each flux exhibit semi-autoregulatory behavior in that flux through each process reduces the standing pool of tRNAs. (B) The governing dynamics of the flux-parity regulatory circuit with key parameters highlighted in blue and flux-parity regulatory components highlighted in red. (C) The steady-state meabolic (purple) and translational (gold) fluxes plotted as a function of the ribosomal allocation under the simple allocation model. Vertical red line indicates the steady-state solution of the flux-parity model under physiological parameter regimes. (D) The steady-state allocation towards ribosomes emerging from flux-parity regulation ($\phi_{Rb}^{(flux-parity)}$) relative to the optimal allocation of the simplistic model ($\phi_{Rb}^{(III)}$) is shown across different parameter regimes for the charging sensitivity τ and the uncharged-tRNA transcription rate κ. Red contour demonstrate the plane of parameter space where the flux-parity regulatory circuit exactly matches the result of optimal allocation. (E) The relative allocation towards ribosomes ($\phi_{Rb}^{(flux-parity)}/\phi_{Rb}^{(III)}$) under physiological parameter regimes plotted as a function of the maximal metabolic rate, ν_{max}.

proteins [77, 78] and has a similar form of

$$\kappa\left(\frac{\text{tRNA}^c}{\text{tRNA}^u}\right) = \kappa_{max}\frac{\frac{\text{tRNA}^c}{\text{tRNA}}}{\frac{\text{tRNA}^c}{\text{tRNA}^u}+\tau}, \tag{2}$$

where κ_{max} represents the maximal rate of tRNA transcription relative to the total biomass.

Numerical integration of this system of equations reveals that the flux-parity regulation is capable of optimizing the allocation towards ribosomes, ϕ_{Rb}, such that the metabolic and translation fluxes are mutually maximized [Fig. 2(C)], thus achieving optimal allocation. Importantly, the optimal behavior inherent to this regulatory mechanism can be attained across a wide range of parameter values for the charging sensitivity τ and the transcription rate κ_{max}, the two key parameters of flux-parity regulation [Fig. 2(D)]. Moreover, the emergent optimal behavior of this regulatory scheme occurs across conditions without the need for any fine-tuning between the flux-parity parameters

and other parameters. For example, the control of allocation via the flux parity regulation matches the optimal allocation (scenario III above) when varying the metabolic rate ν_{max} [Fig. 2(E)].

The theoretical analysis presented in Fig. 2 suggests that a flux-parity regulatory mechanism may be a simple way to ensure optimal ribosomal allocation that is robust to variation in the key model parameters. To test if such a scheme may be implemented in *E. coli*, we compared the behavior of the steady-state flux-parity regulatory circuit within physiological parameter regimes to steady-state measurements of ribosomal allocation and the translation rate as a function of the growth rate [Fig. 3(A & B)]. Remarkably, the predicted steady-state behavior of the flux-parity regulatory circuit describes the observed data with the same quantitative accuracy as the optimal behavior defined by scenario III, as indicated by the overlapping red and blue lines, respectively.

While the flux-parity regulation scheme appears to accurately describe the behavior of *E. coli*, how are metabolic and translational fluxes sensed at a mechanistic level? Many bacteria, including *E. coli*, utilize the small molecule guanosine tetraphosphate (ppGpp) as a molecular indicator of amino acid limitation and has been experimentally shown to regulate ribosomal, metabolic, and tRNA genes [79–82]. Mechanistically, ppGpp levels are enzymatically controlled depending on the metabolic state of the cell, with synthesis being triggered upon binding of an uncharged-tRNA into an actively translating ribosome. While many molecular details of this regulation remain unclear [42, 79–81], the behavior of ppGpp meets all of the criteria of a flux-parity regulator. Rather than explicitly mathematicizing the biochemical dynamics of ppGpp synthesis and degradation, as has been undertaken previously [42, 55, 65], we model the concentration of ppGpp being inversely proportional to the charging balance,

$$[\text{ppGpp}] \propto \frac{\text{tRNA}^u}{\text{tRNA}^c}. \tag{3}$$

This ratio, mathematically equivalent to the odds of a ribosome binding an uncharged-tRNA relative to binding a charged-tRNA, is one example of a biochemically-motivated ansatz that can be considered (Appendix 12.4) and provides a relative measure of the metabolic and translational fluxes.

With this approach, the amount of ppGpp present at low growth rates, and therefore low ribosomal allocation, should be significantly larger than at fast growth rates where ribosomal allocation is larger and charged-tRNA are in abundant supply. While our model cannot make predictions of the *absolute* ppGpp concentration, we can compute the *relative* ppGpp concentration to a reference state $[\text{ppGpp}]_0$ as

$$\frac{[\text{ppGpp}]}{[\text{ppGpp}]_0} = \frac{\frac{\text{tRNA}^u}{\text{tRNA}^c}}{\frac{\text{tRNA}^u_0}{\text{tRNA}^c_0}}. \tag{4}$$

To test this, we compiled and rescaled ppGpp measurements of *E. coli* across a range of growth rates from various literature sources [Fig. 3(C)]. The quantitative agreement between the scaling predicted by Eq. 4 and the experimental measurements strongly suggests that ppGpp assumes the role of a flux-sensor and enforces optimal allocation through the discussed flux-parity mechanism.

The Flux-Parity Allocation Model Predicts E. coli Growth Behavior In and Out Of Steady-State

We find that the flux-parity allocation model is extremely versatile and allows us to quantitatively describe aspects of microbial growth in and out of steady-state and under various physiological stresses and external perturbations with the same core set of parameter. Here, we demonstrate this versatility by comparing predictions to data for four particular examples *using the same self-consistent set of parameters we have used thus far* (Supplementary Table 1). First, we examine the influence of translation-targeting antibiotics like chloramphenicol [Fig. 3(D)] on steady-state growth in different growth media [39, 47]. By incorporating a mathematical description of ribosome inactivation via binding to chloramphenicol (described in Appendix 12), we find that the flux-parity allocation model quantitatively predicts the change in steady-state growth and ribosomal content with increasing chloramphenicol concentration [Fig. 3(E, red shades)]. Furthermore, the effect on the translation speed is qualitatively captured [Fig. 3(F, red shades)]. The ability of the flux-parity allocation model to describe these effects without readjustment of the model and its core parameters is notable and provides a mechanistic rationale for previously established phenomenological relations [39, 47].

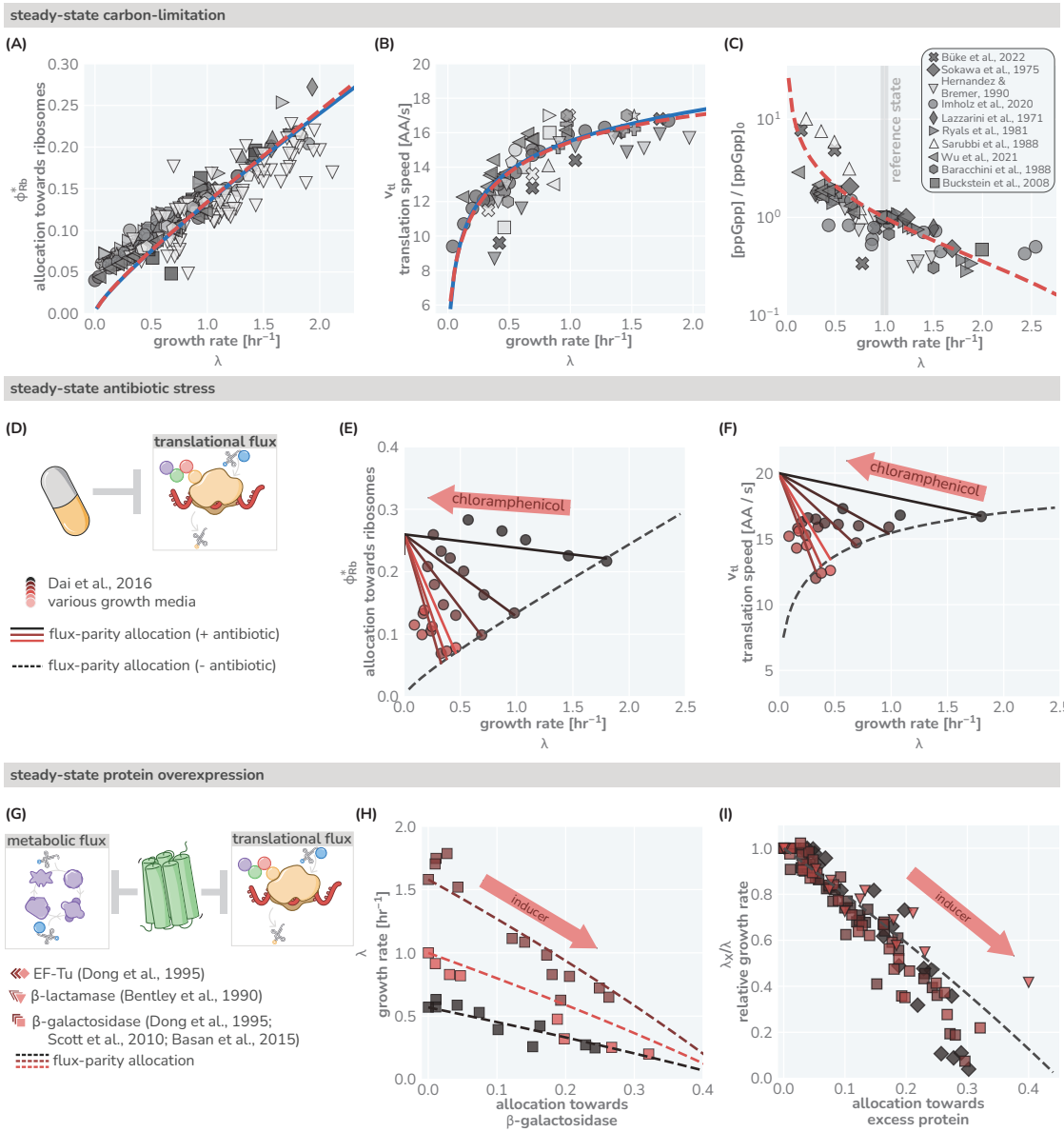

Figure 3: The predictive power of flux-parity regulation in steady-state. Measurements of the (A) ribosomal allocation and the (B) translation rate are plotted alongside the steady-state behavior of the flux-parity regulatory circuit (red dashed line) and the optimal behavior of scenario III (solid blue line). Points and markers are the same as those shown in Fig. 1(F). (C) Measurements of intracellular ppGpp concentrations relative to a reference condition ($\lambda_0 \approx 1$ hr^{-1}) are plotted as a function of growth rate alongside the prediction emergent from the flux-parity regulatory circuit (red dashed line). (D-F) Inhibition of ribosome activity via antibiotic modeled repression of translational flux. Plots show comparison with data for different media (red shades) with the flux-parity model predictions (dashed lines). (G-I) Inhibition of metabolic and translational fluxes through excess gene expression. (H) shows data where β-galactosidase is expressed at different levels. Different shades of red correspond to different growth media. Right-hand panel shows collapse of the growth rates of overexpression of β-galactosidase (squares), β-lactamase (inverted triangles), and EF-Tu (diamonds) relative to the wild-type growth rate in different media conditions. The same set of model parameters listed in Supplementary Table 2 has been used to generate the predictions.

As a second perturbation, we consider the burden of excess protein synthesis by examining the expression of synthetic genes [Fig. 3(G)]. A decrease in growth rate results when cells are forced to synthesize different amounts of the lactose cleaving enzyme β-galactosidase in different media lacking lactose [Fig. 3(H, red shades)]. The flux-parity allocation model (dashed lines) quantitatively predicts the change in growth rate with the measured fraction of β-galactosidase without further fitting (Appendix 12). The trends for different media (red shades) quantitatively collapse onto a single line [Fig. 3(I)] when comparing changes in relative growth rates, a relation which is also captured by the model (dashed black line) and is independent of the overexpressed protein (symbols). This collapse, whose functional form is derived in Appendix 12, demonstrates that the flux-parity allocation model is able to describe excess protein synthesis in general, rather than at molecule- or media-specific level.

As the flux-parity regulatory circuit responds to changes in the metabolic and translational fluxes, it can be used to explore behavior in changing conditions. Consider a configuration where the starting conditions of a culture are tuned such that the ribosomal allocation ϕ_{Rb}, the tRNA charging balance $\text{tRNA}^c/\text{tRNA}^u$, and the ribosome content M_{Rb}/M are set to be above or below the appropriate level for steady-state growth in the environment [Fig. 4(A)]. As the culture grows, the observed ribosomal content M_{Rb}/M is steadily adjusted until the steady-state level is met where it directly matches the optimal allocation [Fig. 4(B)]. This adaptation of the ribosomal content is controlled by dynamic adjustment of the allocation parameters via the flux-parity regulatory circuit [Fig. 4(C)]. To further test the flux-parity allocation model, we examine how accurately this system can predict growth behavior under nutritional shifts [Fig. 4(D-F)]and the entry to starvation [Fig. 4(G-I)].

We first consider a nutrient shift where externally-supplied low-quality nutrients are instantaneously exchanged with rich nutrients. Fig. 4(E) shows three examples of such nutritional upshifts (markers), all of which are well described by the flux-parity allocation theory (dashed lines). The precise values of the growth rates before, during, and after the shift will depend on the specific carbon sources involved. However, by relating the growth rates before and immediately after the shift to the total shift magnitude (as shown in Ref. [58]), one can collapse a large collection of data onto a single curve [Fig. 4(F, markers)]. The collapse emerges naturally from the model (dashed-line) when decomposing the metabolic sector into needed and non-needed components (Appendix 12), demonstrating that the flux-parity allocation model is able to quantitatively describe nutritional upshifts at a fundamental level.

Finally, we consider the growth dynamics during the onset of starvation, another non steady-state phenomenon. Fig. 4(H) shows the growth of batch cultures where glucose is provided as the sole carbon source in different limiting concentrations [83] (markers). The cessation of growth coincides with a rapid, ppGpp-mediated increase in expression of metabolic proteins [79, 84]. Bren *et al.* [83] demonstrated that expression from a glucose-specific metabolic promoter (PtsG) rapidly, yet temporarily, increases with the peak occurring at the moment where growth abruptly stops [Fig. 4(I, solid grey lines)]. The flux-parity allocation model again predicts this behavior [Fig. 4(I, red lines)] without additional fitting (Appendix 12), cementing the ability of the model to describe growth far from steady-state.

Discussion

Microbial growth results from the orchestration of an astoundingly diverse set of biochemical reactions mediated by thousands of protein species. Despite this enormous complexity, experimental and theoretical studies alike have shown that many growth phenotypes can be captured by relatively simple correlations and models which incorporate only a handful of parameters [7, 39, 47, 50, 52, 55, 57, 58, 65]. Through re-examination of these works, we relax commonly invoked approximations and assumptions, include a generalized description of global regulation, and integrate an extensive comparison with data to establish a self-consistent, low-dimensional model of protein synthesis that is capable of quantitatively describing complex growth behaviors in and out of steady-state.

Growth emerges as in previous allocation models [47, 50, 55] as a consequence of protein synthesis and the allocation of ribosome activity towards (i) making new ribosomes, (ii) making the metabolic proteins which sustain the precursors ribosomes require to translate, and (iii) making other proteins cells require to operate. An *optimal allocation* which yields the fastest growth in a given condition is reached when the synthesis of precursors (metabolic flux) and the consumption of precursors (translational flux) are mutually maximized, a process we term *flux-parity regulation*. We analyze how such regulation can be mechanistically achieved by the relative sensing of charged- and uncharged-tRNA via the abundance of a global regulator (such as ppGpp) which diametrically affects the expression

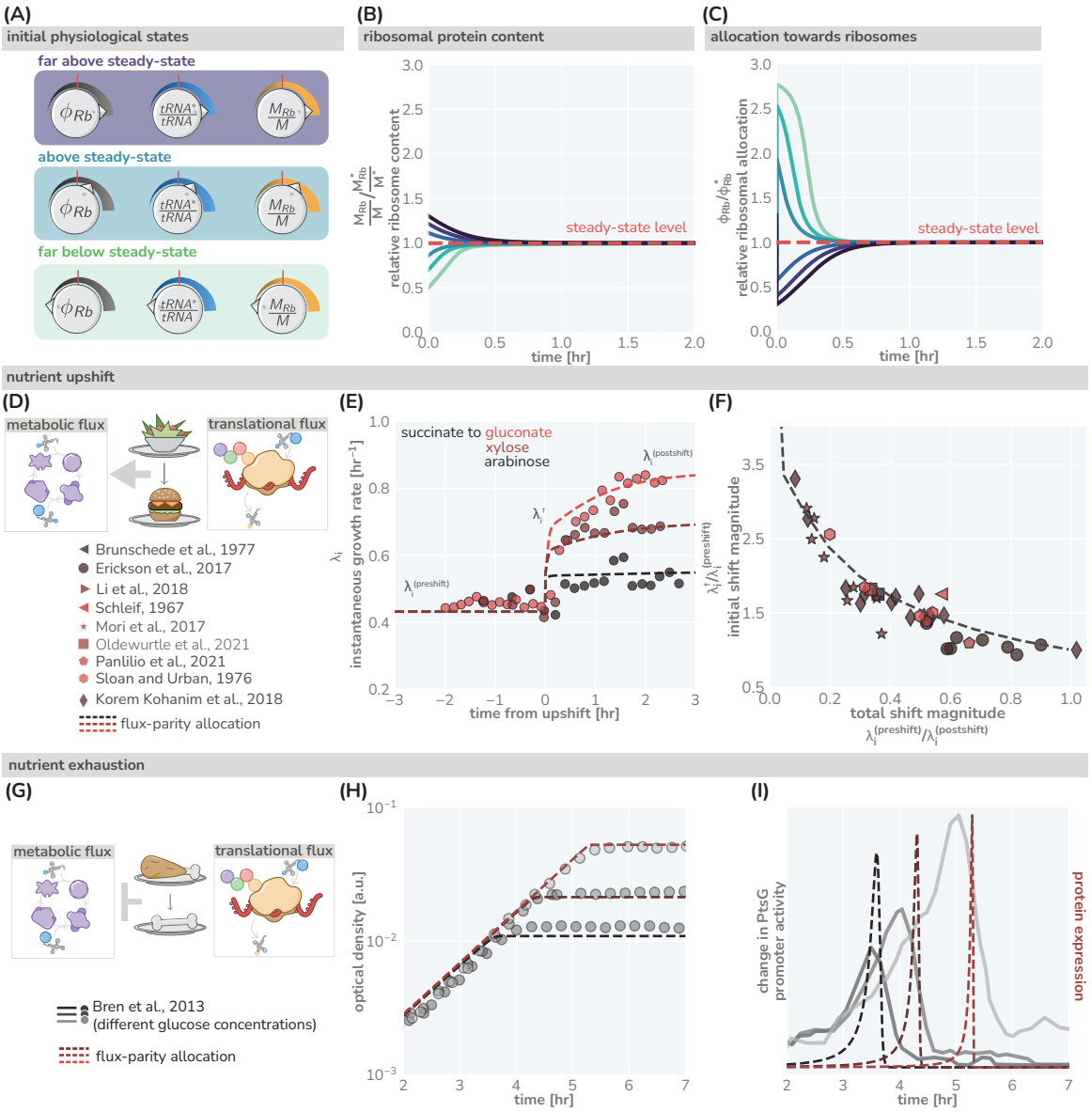

Figure 4: The predictive power of flux-parity regulation out of steady-state. (A) Hypothetical initial configurations of model parameters and variables before begining numerical integration. (B) The equilibration of the ribosomal protein content (M_{Rb}/M). (C) Dynamic adjustment of the ribosomal allocation parameter in response to the new environment. Green and purple colored lines correspond to the initial conditions of the culture from well above to well below the steady-state values, respectively. Dashed red line indicates the steady-state solution. (D-E) Nutrient upshifts with increased metabolic flux. (E) The instantaneous growth rate λ_i for shifts from succinate to gluconate (bright red), xylose (dark red), or arabinose (black) [57]. (F) Collapse of instantaneous growth rate measurements immediately after the shift (relative to the preshift-growth rate) as a function of the total shift magnitude. (G-I) Exhaustion of nutrients in the environment yields a decrease in the metabolic flux, promoting expression of more metabolic proteins. (H) Growth curve measurements in media with different starting concentrations of glucose (0.22 mM, 0.44 mM, and 1.1 mM glucose from light to dark, respectively) overlaid with flux-parity predictions. (I) The change in total metabolic protein synthesis in the flux-parity model (dashed lines) overlaid with the change in expression of a fluorescent reporter from a PtsG promoter (solid lines).

of ribosomal and metabolic genes. Through extensive comparison with 61 data sets from 46 studies, we show that the flux-parity model predicts the fundamental growth behavior of *E. coli* with quantitative accuracy. Beyond the impeccable description of the growth-rate dependent ribosomal content and translation speed across various carbon sources, the flux-parity model quantitatively captures phenomena out of steady-state (including nutrient upshifts and response to starvation) and under externally applied physiological perturbations (such as antibiotic stress or expression of synthetic genes). Notably, the broad agreement across data sets is obtained using a single core parameter set which does not require any adjustment from one scenario to the next. As such, the flux-parity model predicts the microbial "growth laws", providing a mechanistic explanation for previous phenomenological models formulated to understand them [47, 50, 52]. The finding that these predictions hold so well despite the overwhelmingly complex nature of the cell further highlights that biological systems are not irreducibly complex but can be distilled to a small number of fundamental components sufficient to capture the core behavior of the system.

As proteins commonly account for the majority of biomass in microbial organisms and the core processes of protein synthesis are universally conserved among them, it is likely that protein synthesis is a fundamental growth constraint across many organisms. Accordingly, flux-parity regulation may be a very general scheme which ensures the efficient coordination of metabolic and translational fluxes across many microbial organisms. And as our modeling approach is organism agnostic, it should be transferable to a variety of microbes growing in nutrient-replete conditions. Indeed, other organisms including *S. cerevisiae* (Appendix 11) exhibit a strict interdependence between growth rate and ribosome content [18], as is predicted by the flux-parity model. However, more quantitative data on ribosomal content, translation speeds, upshift dynamics, and more need to be acquired to fully examine the commonality of flux-parity regulation in the microbial world.

A common interpretation of previous allocation models is that cells maximize their growth rate in whatever conditions they encounter [49, 65]. Rather, we believe flux-parity regulation only ensures optimal coordination between metabolic and translational fluxes. It does not imply that the growth rate itself is maximized or directly sensed. In particular, the flux-parity model does not assume that the pool of metabolic proteins is tailored to maximize the metabolic flux and thus growth in the encountered conditions. This is in agreement with an expanding body of evidence which shows that microbes frequently synthesize metabolic and other proteins which are not directly needed in the encountered condition and thus impede growth. *E. coli*, for example, synthesizes a plethora of different transport proteins when exposed to poor growth conditions even if the corresponding substrates are not available, collectively occupying a significant portion of the proteome [27, 33, 48, 64]. Accordingly, it has been observed that cells stop synthesizing these proteins when evolving over many generations in the absence of those sugars [85, 86].

But why, then, do we observe an optimal allocation between metabolic and ribosomal proteins when the pool of metabolic proteins itself shows this apparent non-optimal behavior? We posit here that both behaviors emerge from the adaptation to fluctuating conditions: in contrast to the well-defined static conditions of laboratory experiments, the continuous ebb and flow of nutrients in natural environments precludes any sense of stability. Accordingly, the machinery of the cell should be predominantly adapted to best cope with the fluctuating conditions microbial organisms encounter in their natural habitats. A complex regulation of metabolic proteins is thus expected, including for example, the diverse expression of nutrient transporters which promote growth in anticipated conditions, rather than synthesizing only those specific to nutrients that are present in the moment [64].

However, in those fluctuating conditions, flux-parity regulation promotes rapid growth. To illustrate this point, we consider again a nutrient upshift in which there is an instantaneous improvement in the nutrient conditions. We compare the predicted response via flux-parity [Fig. 5 (B, red box)] with that predicted by a simpler step-wise regulation where the allocation solely depends on the environmental condition (and not the internal fluxes) and immediately adjusts to the new steady value at the moment of the shift [Fig. 5 (B, blue box)]. The dynamic reallocation by flux-parity facilitates a sharp increase in the allocation towards ribosomes [Fig. 5(C)], resulting in a rapid increase in instantaneous growth rate compared to the step-wise reallocation mechanism [Fig. 5(D)], suggesting that flux-parity is advantageous in fluctuating environments. As its regulation solely depends on the internal state of the cell (particularly, the relative abundance of charged- to uncharged-tRNA) it holds independently of the encountered conditions. This stands in contrast to the regulation of metabolic proteins, where both the external and internal states dictate what genes are expressed. As a result, optimal coordination between metabolic and translational fluxes occurs ubiquitously across conditions and not only in those that occur in natural habitats

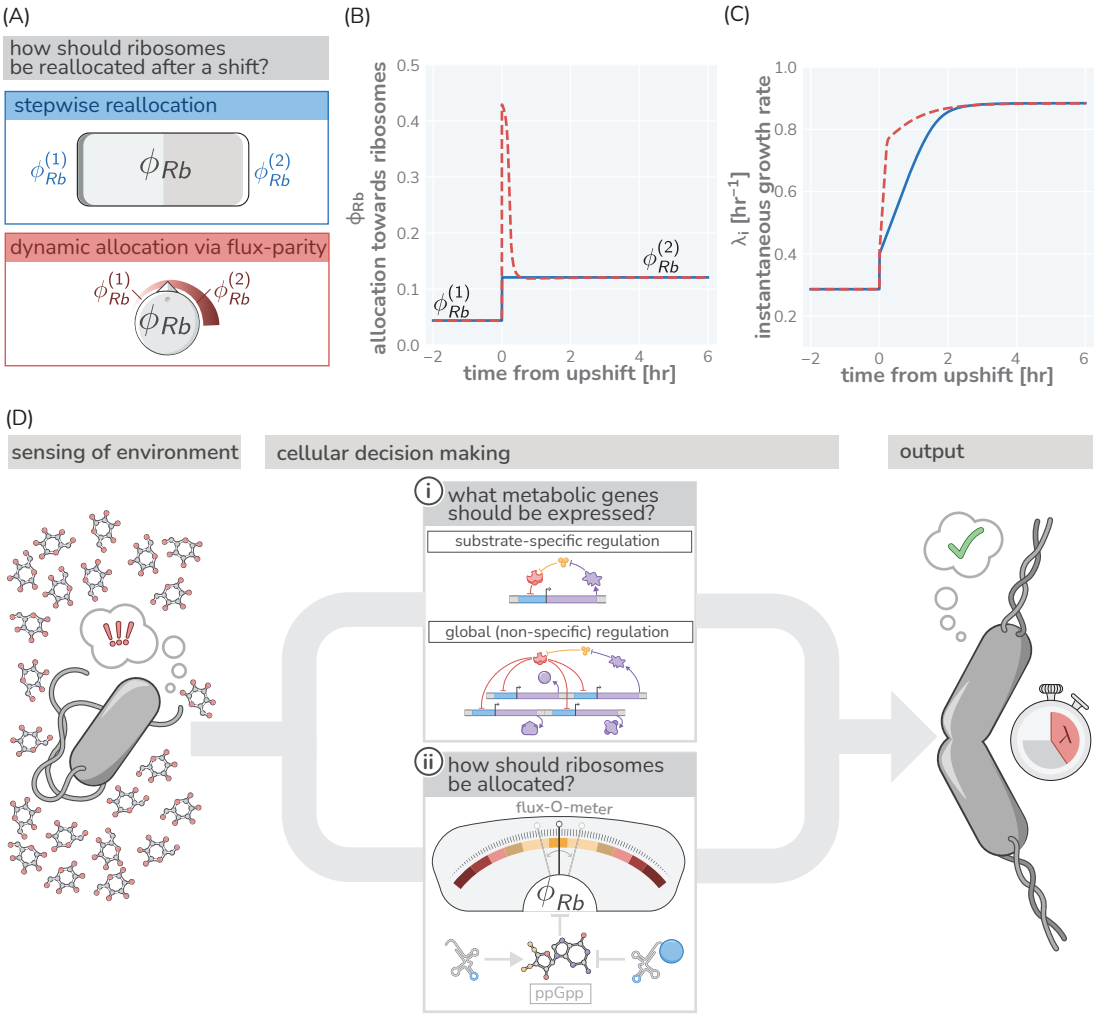

Figure 5: Flux parity allocation as a strategy to adapt to fluctuating conditions. (A) Ribosome reallocation strategies upon a nutrient upshift. After a nutrient upshift, cells either dynamically reallocate their ribosomes given flux-parity regulation (top, red) or they undergo stepwise reallocation from one steady-state value to the next (bottom, blue). (B) The allocation dynamics for both strategies in response to a nutrient upshift. (C) The instantaneous growth rate for both strategies over the course of the shift. Dashed red and solid blue lines correspond to model predictions for optimal allocation and flux-parity regulation, respectively. (D) Cellular decision making in fluctuating environments. Upon sensing features of the environment, cells undergo a two-component decision making protocol defining what metabolic genes should be expressed (top) and how the allocation towards ribosomes should be adjusted to maintain flux-parity. The combination of these processes yield an increase of biomass at a given characteristic growth rate.

and drive adaptation. These broader conditions include steady-state growth within the laboratory, with the "growth laws" observed under those conditions emerging as a serendipitous consequence.

In summary, we view the process of cellular decision making as having two major components [Fig. 5(D)]: (i) determining what metabolic genes should be expressed given the environmental and physiological state and (ii) determining how ribosomes should be allocated given the metabolic and translational fluxes. Flux-parity regulation can explain the latter but many details of the former remain enigmatic. Additional studies are thus required to understand how the regulation of metabolic genes depends on encountered conditions and how it is shaped by adaptation to specific habitats. However, the ability of this theory to predict complex phenotypes across scales suggests that it can also act as a basis to answer these questions, and thereby galvanize an integrative understanding of microbial life connecting physiology, ecology, and evolution.

Data and Code Availability

This work is accompanied by a website (`cremerlab.github.io/flux_parity`) which houses a suite of interactive figures to help the reader gain an intuition for the way the theory operates. Data sets can be downloaded individually from this website. Alternatively, all data and Python code used in this work can be cloned as a GitHub repository (`github.com/cremerlab/flux_parity`). This repository and its releases are also available via Zendodo with the DOI: 10.5281/zenodo.5893800.

Acknowledgments

We thank Uri Alon, Markus Arnoldini, Rachel Banks, Suzy Beeler, Nathan Belliveau, Terence Hwa, Soichi Hirokawa, Christine Jacobs-Wagner, Sergey Kryazhimskiy, Armita Nourmohammad, Manuel Razo-Mejia, Tom Röschinger, Jan Skotheim, Cat Triandafillou, and members of the Tadashi Fukami, Dmitri Petrov, Alfred Spormann, and JC research groups for extensive discussions and the critical reading of the manuscript. GC acknowledges support by the NSF Postdoctoral Research Fellowships in Biology Program (Grant No. 2010807).

References

[1] Jacques Monod. Le taux de croissance en fonction d la concntration de l'aliment dans une population de *Glaucoma piriformis* en culture pure. *Comtes Rendus des Séances de l'Académie des Sciences*, (201):1513–1515, 1935.

[2] Jacques Monod. Ratio d'entretien et ration de croissance dan les populations bactériennes. *Comtes Rendus des Séances de l'Académie des Sciences*, (205):1456–1457, 1937.

[3] Jacques Monod. Sur un phénomene nouveau de croissance complexe dans les cultures bactériennes. *Comptes Rendus des Séances de l'Académie des Sciences*, 212:934–939, 1941.

[4] Jacques Monod. The phenomenon of enzymatic adaptation and its bearings on problems of genetics and cellular differentiation. *Growth Symposium*, 9:223–289, 1947.

[5] Jacques Monod. From enzymatic adaptation to allosteric transitions. *Science*, 154(3748):475–483, October 1966.

[6] Allan Campbell. Synchronization of Cell Division. *Bacteriol Rev*, 21:10, 1957.

[7] M. Schaechter, O. Maaløe, and N. O. Kjeldgaard. Dependency on medium and temperature of cell size and chemical composition during balanced growth of *Salmonella typhimurium*. *Microbiology*, 19(3):592–606, 1958.

[8] N. O. Kjeldgaard, O. Maaløe, and M. Schaechter. The Transition Between Different Physiological States During Balanced Growth of *Salmonella typhimurium*. *Journal of General Microbiology*, 19(3):607–616, December 1958.

[9] Stephen Cooper and Charles E. Helmstetter. Chromosome replication and the division cycle of *Escherichia* coli Br. *Journal of Molecular Biology*, 31(3):519–540, February 1968.

[10] W. D. Donachie, K. J. Begg, and M. Vicente. Cell length, cell growth and cell division. *Nature*, 264(5584):328–333, November 1976.

[11] Suckjoon Jun, Fangwei Si, Rami Pugatch, and Matthew Scott. Fundamental principles in bacterial physiology - history, recent progress, and the future with focus on cell size control: A review. *Reports on Progress in Physics*, 81(5):056601, May 2018.

[12] M Heldal, S Norland, and O Tumyr. X-ray microanalytic method for measurement of dry matter and elemental content of individual bacteria. *Applied and Environmental Microbiology*, 50(5):1251–1257, November 1985.

[13] M. Loferer-Krößbacher, J. Klima, and R. Psenner. Determination of Bacterial Cell Dry Mass by Transmission Electron Microscopy and Densitometric Image Analysis. *Applied and Environmental Microbiology*, 64(2):688–694, February 1998.

[14] Hugh G Lawford and Joyce D Rousseau. Studies on Nutrient Requirements and Cost-Effective Supplements for Ethanol Production by Recombinant E. coli. *Applied Biochemistry and Biotechnology*, 57:20, 1996.

[15] T. G Watson. Amino-acid Pool Composition of *Saccharomyces cerevisiae* as a Function of Growth Rate and Amino-acid Nitrogen Source. *Journal of General Microbiology*, 96(2):263–268, 1976.

[16] R. J. Britten and Clure Ft Mc. The amino acid pool in *Escherichia coli*. *Bacteriol Rev*, 26:292–335, September 1962.

[17] Kirsten Gausing. Regulation of ribosome production in *escherichia* coli: Synthesis and stability of ribosomal RNA and of ribosomal protein messenger RNA at different growth rates. *Journal of Molecular Biology*, 115(3):335–354, September 1977.

[18] Tatiana V. Karpinets, Duncan J. Greenwood, Carl E. Sams, and John T. Ammons. RNA:protein ratio of the unicellular organism as a characteristic of phosphorous and nitrogen stoichiometry and of the cellular requirement of ribosomes for protein synthesis. *BMC Biology*, 4(1):30, September 2006.

[19] Arthur L. Koch. Why can't a cell grow infinitely fast? *Canadian Journal of Microbiology*, 34(4):421–426, April 1988. Publisher: NRC Research Press.

[20] V.J. Hernandez and H. Bremer. Characterization of RNA and DNA synthesis in *escherichia* coli strains devoid of ppGpp. *Journal of Biological Chemistry*, 268(15):10851–10862, May 1993.

[21] B. Magasanik, Adele K. Magasanik, and F. C. Neidhardt. Regulation of Growth and Composition of the Bacterial Cell. In *Ciba Foundation Symposium — Regulation of Cell Metabolism*, pages 334–352. John Wiley & Sons, Ltd, 1959. _eprint: https://onlinelibrary.wiley.com/doi/pdf/10.1002/9780470719145.ch16.

[22] Stephen M. Doris, Deborah R. Smith, Julia N. Beamesderfer, Benjamin J. Raphael, Judith A. Nathanson, and Susan A. Gerbi. Universal and domain-specific sequences in 23S–28S ribosomal RNA identified by computational phylogenetics. *RNA*, 21(10):1719–1730, October 2015.

[23] Chen Davidovich, Matthew Belousoff, Anat Bashan, and Ada Yonath. The evolving ribosome: From non-coded peptide bond formation to sophisticated translation machinery. *Research in Microbiology*, 160(7):487–492, September 2009.

[24] Christian M. Bruell, Carolin Eichholz, Andriy Kubarenko, Virginia Post, Vladimir I. Katunin, Sven N. Hobbie, Marina V. Rodnina, and Erik C. Böttger. Conservation of Bacterial Protein Synthesis Machinery: Initiation and Elongation in Mycobacterium smegmatis. *Biochemistry*, 47(34):8828–8839, August 2008.

[25] Y. Taniguchi, P. J. Choi, G. W. Li, H. Chen, M. Babu, J. Hearn, A. Emili, and X. S. Xie. Quantifying *E. coli* proteome and transcriptome with single-molecule sensitivity in single cells. *Science*, 329:533–8, July 2010.

[26] Bryson D. Bennett, Elizabeth H. Kimball, Melissa Gao, Robin Osterhout, Stephen J. Van Dien, and Joshua D. Rabinowitz. Absolute metabolite concentrations and implied enzyme active site occupancy in *Escherichia* coli. *Nature Chemical Biology*, 5(8):593–599, August 2009.

[27] Alexander Schmidt, Karl Kochanowski, Silke Vedelaar, Erik Ahrné, Benjamin Volkmer, Luciano Callipo, Kèvin Knoops, Manuel Bauer, Ruedi Aebersold, and Matthias Heinemann. The quantitative and condition-dependent *Escherichia coli* proteome. *Nature Biotechnology*, 34(1):104–110, January 2016.

[28] Kaspar Valgepea, Kaarel Adamberg, Andrus Seiman, and Raivo Vilu. *Escherichia coli* achieves faster growth by increasing catalytic and translation rates of proteins. *Molecular BioSystems*, 9(9):2344–2358, July 2013.

[29] Karl Peebo, Kaspar Valgepea, Andres Maser, Ranno Nahku, Kaarel Adamberg, and Raivo Vilu. Proteome reallocation in *Escherichia coli* with increasing specific growth rate. *Molecular BioSystems*, 11(4):1184–1193, 2015.

[30] Gene-Wei Li, David Burkhardt, Carol Gross, and Jonathan S. Weissman. Quantifying absolute protein synthesis rates reveals principles underlying allocation of cellular resources. *Cell*, 157(3):624–635, April 2014.

[31] Rohan Balakrishnan, Matteo Mori, Igor Segota, Zhongge Zhang, Ruedi Aebersold, Christina Ludwig, and Terence Hwa. Principles of gene regulation quantitatively connect DNA to RNA and proteins in bacteria. *bioRxiv*, page 2021.05.24.445329, May 2021.

[32] Matteo Mori, Zhongge Zhang, Amir Banaei-Esfahani, Jean-Benoît Lalanne, Hiroyuki Okano, Ben C Collins, Alexander Schmidt, Olga T Schubert, Deok-Sun Lee, Gene-Wei Li, Ruedi Aebersold, Terence Hwa, and Christina Ludwig. From coarse to fine: The absolute *Escherichia coli* proteome under diverse growth conditions. *Molecular Systems Biology*, 17(5), May 2021.

[33] Nathan M. Belliveau, Griffin Chure, Christina L. Hueschen, Hernan G. Garcia, Jane Kondev, Daniel S. Fisher, Julie A. Theriot, and Rob Phillips. Fundamental limits on the rate of bacterial growth and their influence on proteomic composition. *Cell Systems*, July 2021.

[34] Eyal Metzl-Raz, Moshe Kafri, Gilad Yaakov, Ilya Soifer, Yonat Gurvich, and Naama Barkai. Principles of cellular resource allocation revealed by condition-dependent proteome profiling. *eLife*, 6:e28034, August 2017.

[35] Joao A. Paulo, Jeremy D. O'Connell, Aleksandr Gaun, and Steven P. Gygi. Proteome-wide quantitative multiplexed profiling of protein expression: Carbon-source dependency in *Saccharomyces cerevisiae*. *Molecular Biology of the Cell*, 26(22):4063–4074, November 2015.

[36] Joao A. Paulo, Jeremy D. O'Connell, Robert A. Everley, Jonathon O'Brien, Micah A. Gygi, and Steven P. Gygi. Quantitative mass spectrometry-based multiplexing compares the abundance of 5000 S. *cerevisiae* proteins across 10 carbon sources. *Journal of Proteomics*, 148:85–93, October 2016.

[37] Jianye Xia, Benjamin Sánchez, Yu Chen, Kate Campbell, Sergo Kasvandik, and Jens Nielsen. Proteome allocations change linearly with specific growth rate of *Saccharomyces cerevisiae* under glucose-limitation. Preprint, In Review, May 2021.

[38] Michael Jahn, Vital Vialas, Jan Karlsen, Gianluca Maddalo, Fredrik Edfors, Björn Forsström, Mathias Uhlén, Lukas Käll, and Elton P. Hudson. Growth of Cyanobacteria Is Constrained by the Abundance of Light and Carbon Assimilation Proteins. *Cell Reports*, 25(2):478–486.e8, October 2018.

[39] Xiongfeng Dai, Manlu Zhu, Mya Warren, Rohan Balakrishnan, Vadim Patsalo, Hiroyuki Okano, James R. Williamson, Kurt Fredrick, Yi-Ping Wang, and Terence Hwa. Reduction of translating ribosomes enables *Escherichia* coli to maintain elongation rates during slow growth. *Nature Microbiology*, 2(2):1–9, December 2016.

[40] Markus Basan, Manlu Zhu, Xiongfeng Dai, Mya Warren, Daniel Sévin, Yi-Ping Wang, and Terence Hwa. Inflating bacterial cells by increased protein synthesis. *Molecular Systems Biology*, 11(10):836, October 2015.

[41] Conghui You, Hiroyuki Okano, Sheng Hui, Zhongge Zhang, Minsu Kim, Carl W. Gunderson, Yi-Ping Wang, Peter Lenz, Dalai Yan, and Terence Hwa. Coordination of bacterial proteome with metabolism by cyclic AMP signalling. *Nature*, 500(7462), August 2013.

[42] Chenhao Wu, Rohan Balakrishnan, Matteo Mori, Gabriel Manzanarez, Zhongge Zhang, and Terence Hwa. Cellular perception of growth rate and the mechanistic origin of bacterial growth laws. Preprint, Systems Biology, October 2021.

[43] Francesca Di Bartolomeo, Carl Malina, Kate Campbell, Maurizio Mormino, Johannes Fuchs, Egor Vorontsov, Claes M. Gustafsson, and Jens Nielsen. Absolute yeast mitochondrial proteome quantification reveals trade-off between biosynthesis and energy generation during diauxic shift. *Proceedings of the National Academy of Sciences*, 117(13):7524–7535, March 2020. Publisher: National Academy of Sciences Section: Biological Sciences.

[44] Sophia Hsin-Jung Li, Zhiyuan Li, Junyoung O. Park, Christopher G. King, Joshua D. Rabinowitz, Ned S. Wingreen, and Zemer Gitai. *Escherichia coli* translation strategies differ across carbon, nitrogen and phosphorus limitation conditions. *Nature Microbiology*, 3(8), August 2018.

[45] Tomáš Zavřel, Marjan Faizi, Cristina Loureiro, Gereon Poschmann, Kai Stühler, Maria Sinetova, Anna Zorina, Ralf Steuer, and Jan Červený. Quantitative insights into the cyanobacterial cell economy. *eLife*, 8:e42508, February 2019.

[46] Darren J. Parker, Jean-Benoît Lalanne, Satoshi Kimura, Grace E. Johnson, Matthew K. Waldor, and Gene-Wei Li. Growth-Optimized Aminoacyl-tRNA Synthetase Levels Prevent Maximal tRNA Charging. *Cell Systems*, 11(2):121–130.e6, August 2020.

[47] Matthew Scott, Carl W. Gunderson, Eduard M. Mateescu, Zhongge Zhang, and Terence Hwa. Interdependence of Cell Growth and Gene Expression: Origins and Consequences. *Science*, 330(6007):1099–1102, November 2010.

[48] Sheng Hui, Josh M. Silverman, Stephen S. Chen, David W. Erickson, Markus Basan, Jilong Wang, Terence Hwa, and James R. Williamson. Quantitative proteomic analysis reveals a simple strategy of global resource allocation in bacteria. *Molecular Systems Biology*, 11(2), February 2015.

[49] Benjamin D. Towbin, Yael Korem, Anat Bren, Shany Doron, Rotem Sorek, and Uri Alon. Optimality and sub-optimality in a bacterial growth law. *Nature Communications*, 8(1):14123, April 2017.

[50] Douwe Molenaar, Rogier van Berlo, Dick de Ridder, and Bas Teusink. Shifts in growth strategies reflect tradeoffs in cellular economics. *Molecular Systems Biology*, 5(1):323, January 2009.

[51] Jonathan R. Karr, Jayodita C. Sanghvi, Derek N. Macklin, Miriam V. Gutschow, Jared M. Jacobs, Benjamin Bolival, Nacyra Assad-Garcia, John I. Glass, and Markus W. Covert. A Whole-Cell Computational Model Predicts Phenotype from Genotype. *Cell*, 150(2):389–401, July 2012.

[52] M. Scott, S. Klumpp, E. M. Mateescu, and T. Hwa. Emergence of robust growth laws from optimal regulation of ribosome synthesis. *Molecular Systems Biology*, 10(8):747–747, August 2014.

[53] Andrea Y. Weiße, Diego A. Oyarzún, Vincent Danos, and Peter S. Swain. Mechanistic links between cellular trade-offs, gene expression, and growth. *Proceedings of the National Academy of Sciences of the United States of America*, 112(9):E1038–1047, March 2015.

[54] Arijit Maitra and Ken A. Dill. Bacterial growth laws reflect the evolutionary importance of energy efficiency. *Proceedings of the National Academy of Sciences of the United States of America*, 112(2):406–411, January 2015.

[55] Nils Giordano, Francis Mairet, Jean-Luc Gouzé, Johannes Geiselmann, and Hidde de Jong. Dynamical Allocation of Cellular Resources as an Optimal Control Problem: Novel Insights into Microbial Growth Strategies. *PLOS Computational Biology*, 12(3):e1004802, March 2016.

[56] Matteo Mori, Severin Schink, David W. Erickson, Ulrich Gerland, and Terence Hwa. Quantifying the benefit of a proteome reserve in fluctuating environments. *Nature Communications*, 8(1), October 2017.

[57] David W. Erickson, Severin J. Schink, Vadim Patsalo, James R. Williamson, Ulrich Gerland, and Terence Hwa. A global resource allocation strategy governs growth transition kinetics of *Escherichia coli*. *Nature*, 551(7678):119–123, November 2017.

[58] Yael Korem Kohanim, Dikla Levi, Ghil Jona, Benjamin D. Towbin, Anat Bren, and Uri Alon. A Bacterial Growth Law out of Steady State. *Cell Reports*, 23(10):2891–2900, June 2018.

[59] Derek N. Macklin, Travis A. Ahn-Horst, Heejo Choi, Nicholas A. Ruggero, Javier Carrera, John C. Mason, Gwanggyu Sun, Eran Agmon, Mialy M. DeFelice, Inbal Maayan, Keara Lane, Ryan K. Spangler, Taryn E. Gillies, Morgan L. Paull, Sajia Akhter, Samuel R. Bray, Daniel S. Weaver, Ingrid M. Keseler, Peter D. Karp, Jerry H. Morrison, and Markus W. Covert. Simultaneous cross-evaluation of heterogeneous *e. coli* datasets via mechanistic simulation. *Science*, 369(6502), July 2020.

[60] Xiao-Pan Hu, Hugo Dourado, Peter Schubert, and Martin J. Lercher. The protein translation machinery is expressed for maximal efficiency in *Escherichia* coli. *Nature Communications*, 11(1):5260, October 2020.

[61] Hugo Dourado and Martin J. Lercher. An analytical theory of balanced cellular growth. *Nature Communications*, 11(1):1226, March 2020. Number: 1 Publisher: Nature Publishing Group.

[62] Anjan Roy, Dotan Goberman, and Rami Pugatch. Transcription-translation machinery – an autocatalytic network coupling all cellular cycles and generating a plethora of growth laws. *arXiv:2103.15356 [physics, q-bio]*, March 2021.

[63] Diana Serbanescu, Nikola Ojkic, and Shiladitya Banerjee. Nutrient-Dependent Trade-Offs between Ribosomes and Division Protein Synthesis Control Bacterial Cell Size and Growth. *Cell Reports*, 32(12), September 2020.

[64] Rohan Balakrishnan, Roshali T de Silva, Terence Hwa, and Jonas Cremer. Suboptimal resource allocation in changing environments constrains response and growth in bacteria. *Molecular Systems Biology*, 17(12):e10597, December 2021. Publisher: John Wiley & Sons, Ltd.

[65] Evert Bosdriesz, Douwe Molenaar, Bas Teusink, and Frank J. Bruggeman. How fast-growing bacteria robustly tune their ribosome concentration to approximate growth-rate maximization. *The FEBS journal*, 282(10):2029–2044, May 2015.

[66] Francis Mairet, Jean-Luc Gouzé, and Hidde de Jong. Optimal proteome allocation and the temperature dependence of microbial growth laws. *npj Systems Biology and Applications*, 7(1):1–11, March 2021.

[67] Gordon Churchward, Hans Bremer, and Ry Young. Macromolecular composition of bacteria. *Journal of Theoretical Biology*, 94(3):651–670, February 1982.

[68] Francisco Feijó Delgado, Nathan Cermak, Vivian C. Hecht, Sungmin Son, Yingzhong Li, Scott M. Knudsen, Selim Olcum, John M. Higgins, Jianzhu Chen, William H. Grover, and Scott R. Manalis. Intracellular Water Exchange for Measuring the Dry Mass, Water Mass and Changes in Chemical Composition of Living Cells. *PLOS ONE*, 8(7):e67590, July 2013. Publisher: Public Library of Science.

[69] A. H. Stouthamer. A theoretical study on the amount of ATP required for synthesis of microbial cell material. *Antonie van Leeuwenhoek*, 39(1):545–565, December 1973.

[70] Pranas Grigaitis, Brett G. Olivier, Tomas Fiedler, Bas Teusink, Ursula Kummer, and Nadine Veith. Protein cost allocation explains metabolic strategies in *Escherichia* coli. *Journal of Biotechnology*, 327:54–63, February 2021.

[71] Chalongrat Noree, Kyle Begovich, Dane Samilo, Risa Broyer, Elena Monfort, and James E. Wilhelm. A quantitative screen for metabolic enzyme structures reveals patterns of assembly across the yeast metabolic network. *Molecular Biology of the Cell*, 30(21):2721–2736, October 2019.

[72] K. A. Dill, K. Ghosh, and J. D. Schmit. Physical limits of cells and proteomes. *Proceedings of the National Academy of Sciences*, 108(44):17876–17882, November 2011.

[73] Moshe Kafri, Eyal Metzl-Raz, Felix Jonas, and Naama Barkai. Rethinking cell growth models. *FEMS Yeast Research*, 16(7):fow081, November 2016.

[74] Ludovico Calabrese, Jacopo Grilli, Matteo Osella, Christopher P. Kempes, Marco Cosentino Lagomarsino, and Luca Ciandrini. Role of protein degradation in growth laws. Technical report, August 2021. Company: Cold Spring Harbor Laboratory Distributor: Cold Spring Harbor Laboratory Label: Cold Spring Harbor Laboratory Section: New Results Type: article.

[75] Michael Jahn, Nick Crang, Markus Janasch, Andreas Hober, Björn Forsström, Kyle Kimler, Alexander Mattausch, Qi Chen, Johannes Asplund-Samuelsson, and Elton Paul Hudson. Protein allocation and utilization in the versatile chemolithoautotroph Cupriavidus necator. *eLife*, 10:e69019, November 2021. Publisher: eLife Sciences Publications, Ltd.

[76] Albert L. Müller, Wenyu Gu, Vadim Patsalo, Jörg S. Deutzmann, James R. Williamson, and Alfred M. Spormann. An alternative resource allocation strategy in the chemolithoautotrophic archaeon *Methanococcus maripaludis*. *Proceedings of the National Academy of Sciences*, 118(16), April 2021.

[77] A. C. Skjold, H. Juarez, and C. Hedgcoth. Relationships among deoxyribonucleic acid, ribonucleic acid, and specific transfer ribonucleic acids in *escherichia* coli 15T - at various growth rates. *Journal of Bacteriology*, 115(1):177–187, July 1973.

[78] Hengjiang Dong, Lars Nilsson, and Charles G. Kurland. Co-variation of tRNA Abundance and Codon Usage in *escherichia* coli at Different Growth Rates. *Journal of Molecular Biology*, 260(5):649–663, August 1996.

[79] Lisa U. Magnusson, Anne Farewell, and Thomas Nyström. ppGpp: a global regulator in *Escherichia coli*. *Trends in Microbiology*, 13(5):236–242, May 2005.

[80] Brent W. Anderson, Danny K. Fung, and Jue D. Wang. Regulatory Themes and Variations by the Stress-Signaling Nucleotide Alarmones (p)ppGpp in Bacteria. *Annual Review of Genetics*, 55(1), 2021. _eprint: https://doi.org/10.1146/annurev-genet-021821-025827.

[81] Katarzyna Potrykus and Michael Cashel. (p)ppGpp: Still Magical? *Annual Review of Microbiology*, 62(1):35–51, 2008. _eprint: https://doi.org/10.1146/annurev.micro.62.081307.162903.

[82] Katarzyna Potrykus, Helen Murphy, Nadège Philippe, and Michael Cashel. ppGpp is the major source of growth rate control in E. coli. *Environmental microbiology*, 13(3):563–575, March 2011.

[83] Anat Bren, Yuval Hart, Erez Dekel, Daniel Koster, and Uri Alon. The last generation of bacterial growth in limiting nutrient. *BMC Systems Biology*, 7(1):27, March 2013.

[84] Patrick P. Dennis, Mans Ehrenberg, and Hans Bremer. Control of rRNA Synthesis in *escherichia* coli: a Systems Biology Approach. *Microbiology and Molecular Biology Reviews*, 68(4):639–668, December 2004.

[85] Nicholas Leiby and Christopher J. Marx. Metabolic Erosion Primarily Through Mutation Accumulation, and Not Tradeoffs, Drives Limited Evolution of Substrate Specificity in *Escherichia coli*. *PLOS Biology*, 12(2):e1001789, February 2014.

[86] John S. Favate, Shun Liang, Srujana S. Yadavalli, and Premal Shah. The landscape of transcriptional and translational changes over 22 years of bacterial adaptation. *bioRxiv*, page 2021.01.12.426406, January 2021. Publisher: Cold Spring Harbor Laboratory Section: New Results.

Supplementary Figures

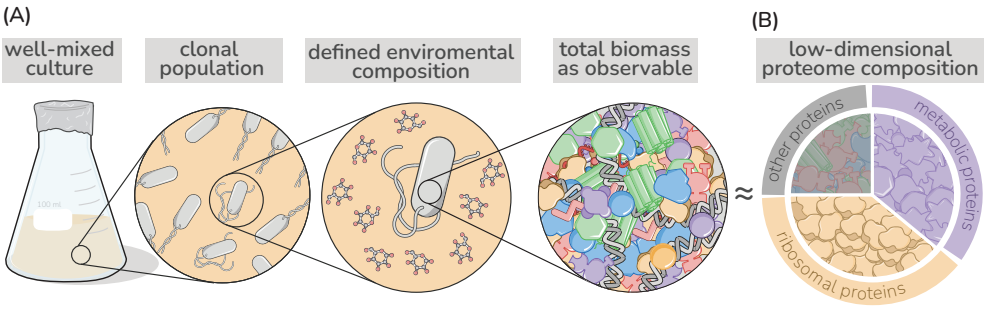

Supplementary Figure 1: Coarse grained description of biomass and the proteome Low-dimensional allocation models consider in their simplest form growth of a clonal population within a well-mixed environment. Biomass is described in a highly simplified manner focusing in the simplest case on protein synthesis alone [50, 52], with different protein species jointly considered by a few different protein classes. Here, metabolic proteins (purple), ribosomal proteins (gold), or "other" proteins (gray).

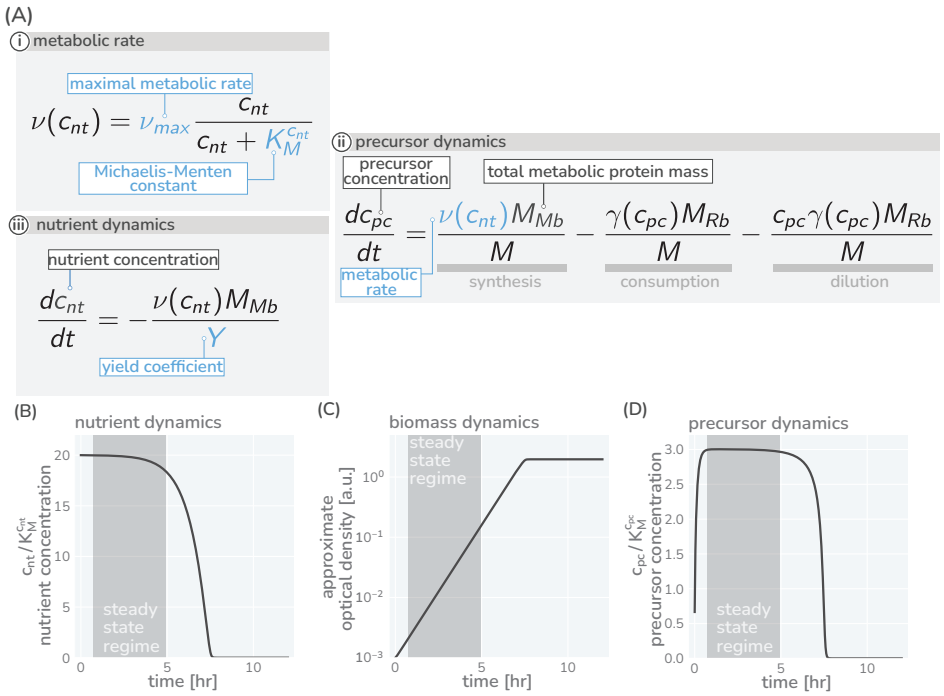

Supplementary Figure 2: Precursor synthesis and growth when nutrients are not saturating. In general, the environmental conditions microbes encounter changes rapidly and nutrient availability commonly limits growth. Growing batch cultures, fox example run out of nutrients eventually and growth stops. The allocation modeling framework can account such a dynamics by including metabolic rates which depend on the nutrient concentrations in the environment. In the simplest case, one nutrient source is considered (concentration n) with the metabolic rate $\nu(n)$ depending on the concentration in a Michaelis-Menten manner with a maximal metabolic rate being reached only at high nutrient concentrations (A,i). The dynamics of precursors is given by a balance of synthesis, consumption, and dilution (A,ii), replacing the corresponding equation of the simple model in [Fig. 1(B,iv)]. The modeling of growth further requires the explicit modeling of nutrient concentrations. This dynamics depends on the specifics of the environment and, depending on the environment, can become very complex with multiple sources and sinks affecting the nutrient concentration. Here, we consider a typical batch culture scenario in which cells grow under well-mixed conditions. Nutrients are provided only initially and nutrient concentrations are falling because of consumption (A,iii). (B-D) Resulting temporal variation of nutrient concentrations (C), biomass accumulation (D), and precursor concentration (E) when integrating the model equations and using a parameter set descriptive of *E. coli* growing in a glucose-minimal medium with a growth rate ≈ 1 hr^{-1} and a starting glucose concentration of $10mM$. As experimentally observed, initially abundant nutrients are consumed and biomass accumulates (exponential phase) until nutrients are exhausted and growth stops (saturation phase) (B and C). Importantly, precursor concentrations (D) quickly reach a constant plateau which lasts until nutrients become scare ($c_{nt} \gg K_M^{c_{nt}}$ and $\nu(c_{nt}) \approx \nu_{max}$). During this transient period (shaded regions) the synthesis of precursors matches the consumption by protein synthesis and dilution, meaning $\frac{dc_{pc}}{dt} = 0$. Given a constant precursor concentration c_{pc}^*, the translation rate $\gamma(c_{pc}^*)$ is also constant. As a consequence, the protein pool approaches a steady composition dictated by the allocation parameters ($\frac{M_{Rb}}{M} = \phi_{Rb}$, $\frac{M_{Mb}}{M} = \phi_{Mb}$ and $\frac{M_O}{M} = \phi_O$). With precursor concentrations and protein composition remaining constant, the system is in a *steady-state* and biomass accumulates exponentially over time, $\frac{dM}{dt} = \gamma(c_{pc}^*)\phi_{Rb} M \equiv \lambda M$. This is the steady state regime we focus on in the main text. Note that the steady state growth regime readily emerges when we consider dilution (see Supplementary 6). Model parameters are provided in Supplemental Table 1. Biomass units are converted to optical density assuming at $OD_{600nm} = 1$, there are 10^9 cells per mL and 10^9 amino acids per cell. An interactive version of these dynamics can be found on the paper website.

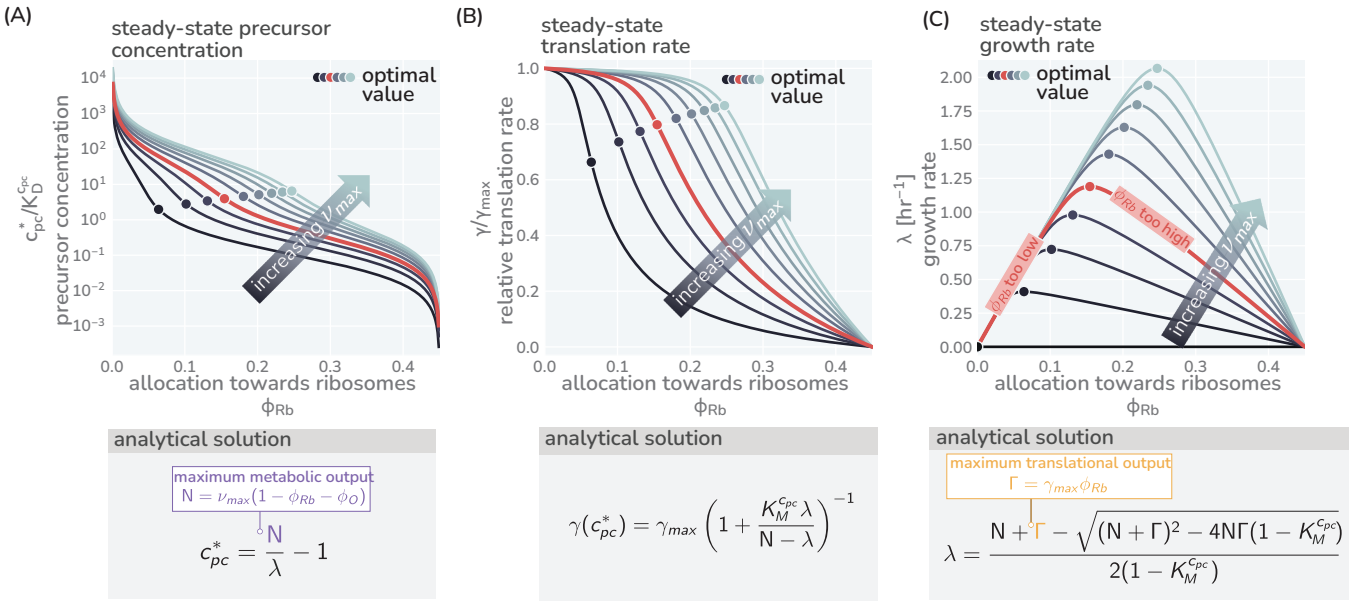

Supplementary Figure 3: Modeling predictions of steady growth behavior. (A) Variation of the precursor concentration with varying allocation parameters (ϕ_R) and maximal metabolic rate (ν_{max}). (B C) Corresponding trends of translation and growth rate as also shown in Fig. 1 (C) and (D). Corresponding boxes show the analytical expression describing the steady-state precursor concentration, translation speed, and growth rate with details of the derivation provided in Appendix 7. Used model parameters provided in Supplementary Table 1. Colors indicate different metabolic rates ν_{max}= 0.2 - 12.5 hr^{-1}.

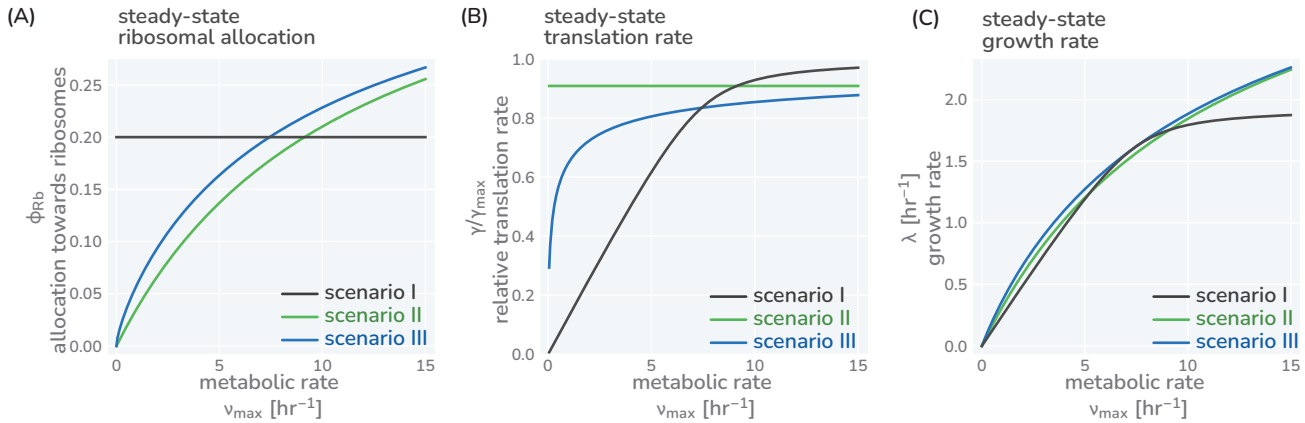

Supplementary Figure 4: Three different allocation scenarios. The variation of precursor concentration (A), translation rate (B), and growth rate (C) with changing metabolic rate is shown for the three allocation scenarios introduced in the main text; fixed allocation (scenario I, black lines), prioritizing fast translation (scenario II, green lines), and growth-optimal allocation (scenario III, blue lines). Plotted are the analytical solutions provided in Fig. 1(E) and derived in Appendix 7. The resulting relations between growth rate and translation as well as growth rate and ribosome content are shown in Figure 1(G,H). We here discuss the consequence of these allocation scenarios in more detail. *Scenario I - fixed allocation*: In this scenario, allocation is fixed and does not vary with conditions. Locking in the ribosome allocation to $\phi_{Rb} = 0.25$ (A, black line), for example, carries strong consequences for translation and growth rates (B and C, black lines). When conditions are poor (ν_{max} is small), the translation rate is significantly lower than the maximal rate as there are too many ribosomes competing for a small pool of precursors (B). The translation and growth rates increase with the metabolic rate ν_{max} until the influx of precursors is sufficiently high such that all ribosomes are translating close to their maximum and growth-rate is at its optimal value. Further increasing the metabolic rate does not increase the growth rate [plateau of black curve in (B)] as all ribosomes are already translating close to their maximum rate. *Scenario II - prioritizing fast translation*: In this scenario, allocation is adjusted such that translation rates are maintained at a high value. This is achieved by tuning the allocation between ribosomes and metabolic proteins such that a constant precursor concentration $c^*_{pc} \gg K_M^{c_{pc}}$ is maintained. For example, at higher metabolic rates, the metabolic proteins can sustain a higher influx of precursors allowing a larger allocation towards ribosomal proteins ϕ_R (green lines). *Scenario III - optimizing growth*: In this scenario, allocation is tuned to optimize growth rate across conditions, meaning that the fastest growth rate is achieved given a set metabolic rate and other model parameters. For example, the allocation towards ribosomes ϕ_{Rb} is adjusted with the metabolic rate such that the growth rate rests at the peak of the curves shown in Fig. 1(C) (blue lines). Accordingly, the growth rate continues to increase with higher metabolic rates always exceeding the growth rate of scenario I and II (C, green line)]. Model parameters follow the reference set for *E. coli* (Supplementary Table 1). Black lines correspond to a constant allocation $\phi_{Rb}^{(I)} = 0.20$ and green lines correspond to a constant precursor concentration $c^*_{pc} \approx 10 K_M^{c_{pc}}$, yielding a constant translation rate of $\gamma(c^*_{pc}) \approx 0.9\gamma_{max}$. An interactive version of these figure panels is available on the paper website.